2020

Selective adsorption of rare earth ions from aqueous solution on metal-organic framework HKUST-1

Liang Zhao

Xiaoguang Duan

Muhammad R. A. Azhar
Edith Cowan University

Hongqi Sun
Edith Cowan University

Xiangchen Fang

See next page for additional authors

10.1016/j.ceja.2020.100009

Zhao, L., Duan, X., Azhar, M. R., Sun, H., Fang, X., & Wang, S. (2020). Selective adsorption of rare earth ions from aqueous solution on metal-organic framework HKUST-1. *Chemical Engineering Journal Advances, 1*, article 100009. https://doi.org/10.1016/j.ceja.2020.100009

Chemical Engineering Journal Advances 1 (2020) 100009

Contents lists available at ScienceDirect

Chemical Engineering Journal Advances

journal homepage: www.elsevier.com/locate/ceja

Selective adsorption of rare earth ions from aqueous solution on metal-organic framework HKUST-1

Liang Zhao[a,b], Xiaoguang Duan[c], Muhammad R. Azhar[b], Hongqi Sun[d], Xiangchen Fang[a], Shaobin Wang[c,*]

[a] Fushun Research Institute of Petroleum and Petrochemicals, SINOPEC, Fushun 113001, China
[b] WASM:Minerals, Energy and Chemical Engineering, Curtin University, GPO Box U1987, Perth, WA 6845, Australia
[c] School of Chemical Engineering and Advanced Materials, The University of Adelaide, Adelaide, SA 5005, Australia
[d] School of Engineering, Edith Cowan University, 270 Joondalup Drive, Joondalup, Perth, WA 6027, Australia

ARTICLE INFO

Keywords:
HKUST-1
Cerium (III)
Lanthanum (III)
Metal-organic framework
Adsorption

ABSTRACT

Recovery of rare earth ions from wastewater holds an important strategy for the use of the precious resources. In this study, we found that a metal-organic framework (MOF), HKUST-1, exhibited a high affinity and selectivity towards adsorptive recovery of rare earth ions (Ce^{3+} and La^{3+}) in aqueous solutions. The adsorbent showed a remarkable adsorption capacity of 234 mg/g and 203 mg/g for Ce^{3+} and La^{3+} at pH = 6, respectively. More importantly, its adsorption selectivity of the rare earth ions was about 87% against other metal ions. The adsorption isotherm, kinetics, and mechanism in the process were also investigated. The adsorption process can be better fit by the Freundlich model in isotherm and the pseudo-second-order model in kinetics. A plausible mechanism for the adsorption of metal ions on the HKUST-1 was proposed by considering ion exchange and the covalent bonding between the adsorbent and metal ions. The selectivity can be attributed to the different bonding abilities to metal ions.

1. Introduction

Rare earth elements (REEs) such as lanthanum and cerium, which can be used in numerous high-tech devices, are of critically low reserves on the Earth [1–5]. With the increasing demand of REEs, more and more effluents of them from the processes of mining, stacking and purification have been discharged into the environment [6–10]. This not only wastes the resources, but also causes serious water pollution. Therefore, it is necessary to explore an effective way to extract REEs from the waste streams. Among various methods, adsorption holds considerable promises because of the low-cost operation and efficient capture ability [11,12]. Porous materials, for examples, activated carbon, alumina, zeolite and biomass, have demonstrated competing performances for adsorption. However, these traditional adsorbents are limited by either a lower adsorption capacity or poor selectivity.

Recently, considerable research interests have been focused on crystalline porous materials, metal-organic frameworks (MOFs), which have a tailored pore structure with a ultra-high surface area by the different configurations of organic and metallic components [13,14]. On the basis of these characteristics, MOFs have been used for a variety of applications including gas storage and separation [15–17], drug delivery [18–20], catalysis [21–23], sensing [24–26] and elimination of heavy metal ions [27–29].

HKUST-1 is one of the widely studied MOF materials. Also, it is commercially available, and thus has been widely used in gas adsorption and removal of aqueous pollutants [15, 30–32]. However, few works have focused on the adsorption capacity of rare earth ions on HKUST-1, especially for the selective adsorption of rare earth ions from the mixed solution with a variety of metal ions. Generally, rare earth ions are always in company with other metal ions during the process of mining [6], so selective adsorption of the rare earth ions is of high importance and practical values.

In our previous study [33], a HKUST-1 was tested in single Ce^{3+} ion solution for the adsorption mechanism and reusability, while the effect of associated metal ions on the adsorption of rare earth ions (such as Ce^{3+} and La^{3+}) was not examined. In the present work, we prepared HKUST-1 by a new solvothermal method and systematically investigated its selective adsorption behavior towards REEs in a solution with multiple ions. Based on the real mining situation, diverse metal ions with different valence states were selected as the interference ions, and high adsorption selectivity of REEs on HKUST-1 was achieved. Adsorption kinetics and equilibrium isotherm were determined at different conditions by varying the contact time, initial concentration of the REEs, and

* Corresponding author.
E-mail address: shaobin.wang@adelaide.edu.au (S. Wang).

https://doi.org/10.1016/j.ceja.2020.100009
Received 13 June 2020; Received in revised form 28 July 2020; Accepted 29 July 2020

solution pH. It was found that HKSUT-1 demonstrated fast removal kinetics and a high selective adsorption capacity of REEs.

2. Experimental

2.1. Chemicals and HKUST-1 synthesis

Most of the chemicals including trimesic acid (H_3BTC), copper (II) nitrate trihydrate ($Cu(NO_3)_2•3H_2O$), zinc nitrate hexahydrate ($Zn(NO_3)_2•6H_2O$), lanthanum (III) nitrate hexahydrate ($La(NO_3)_3•6H_2O$), cerium (III) chloride heptahydrate ($CeCl_3•7H_2O$), magnesium chloride hexahydrate ($MgCl_2•6H_2O$), *N,N*-dimethylformamide (DMF), hydrochloric acid (37%), sodium hydroxide, and methanol were obtained from Sigma-Aldrich. These chemicals are in a high purity and used without further purification. For the preparation of solutions, ultrapure water obtained from a Hydro-Check 414R purification system (18 MΩ cm) was used.

HKUST-1 synthesis was carried out by a reported solvothermal method with some modifications [15]. For the preparation, $Cu(NO_3)_2•3H_2O$ (1.5 g), H_3BTC (0.75 g) and DMF (37.5 mL) were well mixed by stirring and then transferred into a Teflon-lined steel autoclave (100 mL), which was heated in a convection oven to 75 ˚C and maintained for 24 h. After filtration and DMF washing for three times, crystalline precipitates were collected and further treated by immersing in a DMF solution (50 mL) for 8 h. The final product was obtained by separation and drying at 150 ˚C for 12 h in a vacuum oven.

2.2. Characterizations

The crystalline structure of the HKUST-1 was determined by powder X-ray diffraction (XRD) from 5 to 40˚ (0.02˚ per step) using a diffractometer of D8 Advance-Bruker aXS with Cu Kα radiation ($\lambda = 1.5406$ Å). Surface morphology was investigated by scanning electron microscopy (SEM) on a Zeiss SUPRA^{TM} 55VP and element mapping was attained from a Horiba Emax energy dispersive X-ray spectrometer (EDS). The surface functionalities were checked by a Perkin Elmer FT-IR Spectrum 100 using an attenuated total reflectance technique in a range of 4000 - 650 cm^{-1}. The Raman spectra were determined on a Renishaw Raman microscope at room temperature using a laser with an excitation wavelength of 785 nm. X-ray photoelectron spectroscopy (XPS) was performed with an Al Kα X-ray source on a Thermo Escalab 250.

The surface area and porosity of HKUST-1 samples were examined by a nitrogen adsorption analyzer (Micromeritics, TriStar II PLUS). Before the adsorption, the samples were subjected to vacuum purification at 150 ˚C for 12 h. Thermogravimetric analysis of fresh and regenerated samples was also conducted using a TGA/DSC1 STAR^e system from METTLER TOLEDO, USA. For the analysis, an argon gas was flown at 10 mL/min in the furnace, which was heated at a rate of 10 ˚C/min to 700 ˚C. After the adsorption, metal leaching in the solution was determined on a PerkinElmer, Optima 8300 equipment of inductively coupled plasma optical emission spectrometry (ICP-OES). The zeta potential of HKUST-1 in ultrapure water was measured on a zeta potential analyzer (Malvern Instrument Co., ZEN 2010, UK).

2.3. Adsorption tests

Stock solutions of Mg^{2+}, La^{3+}, Ce^{3+}, Zn^{2+}, Co^{2+} and Cr^{3+} were prepared from $MgCl_2•6H_2O$, $La(NO_3)_3•6H_2O$, $CeCl_3•7H_2O$, $Zn(NO_3)_2•6H_2O$, $Co(NO_3)_2•6H_2O$ and $Cr(NO_3)_2•9H_2O$ at a concentration of 1000 mg/L by dissolution of the corresponding salts in ultrapure water. For batch adsorption tests, the stock solution was diluted at different concentrations of 100 mL solution and mixed with 100 mg of adsorbents. The mixture solution was put in a temperature-controlled shaker at 25 ˚C with an agitation speed of 150 rpm. After the period of equilibrium, some solutions were withdrawn and centrifuged for 5 min. The concentrations of Ce^{3+}, La^{3+}, Zn^{2+}, Mg^{2+}, Cu^{2+}, Co^{2+} and Cr^{3+} in clean solutions were determined by ICP-OES.

For the effect of solution pH, the initial solution pHs were adjusted between 2 and 6 using 0.1 mol/L HCl or NaOH, due to REE precipitation at pH>6 [12]. For kinetic investigation, the adsorption runs were conducted within a period of time, 30 - 480 min. For adsorption isotherms of Ce^{3+}, La^{3+}, Zn^{2+}, Mg^{2+}, Co^{2+} and Cr^{3+}, the tests were run at varying concentrations up to 1000 mg/L. The ion removal efficiency (η, %), selectivity (s, %) and adsorption capacity (q_t, mg/g) were calculated according to the following equations, (1), (2) and (3), respectively.

$$\eta = (C_0 - C_t)/C_0 \times 100\% \quad (1)$$

$$s = q_{REE}/q_{total} \quad (2)$$

$$q_t = (C_0 - C_t)V/m \quad (3)$$

where, C_0 and C_t are the initial and residual concentrations of Ce^{3+}, La^{3+}, Zn^{2+}, Mg^{2+} Co^{2+} and Cr^{3+} in the solution, respectively. q_{REE} is the adsorption quantity of Ce^{3+} and La^{3+}, while q_{total} is the adsorption quantity of all metal ions. q_t is the ion adsorption quantity (mg/g) at time t, V is the solution volume (L), and m is the weight of HKUST-1 adsorbents (g).

The crystalline stability of HKUST-1 in water was checked. The conditions were maintained similarly to the batch adsorption tests. After the equilibrium period, the solid sample was collected by a centrifuge and the water solution was analyzed by ICP-OES for Cu^{2+} concentration.

After adsorption, HKUST-1 with adsorbed Ce^{3+}, La^{3+}, Zn^{2+} and Mg^{2+} was tested for their desorption and reuse. The solid samples were immersed in 80 mL of methanol for 12 h and then separated by filtration. After washing with ultrapure water, the adsorbent solid was dried at 150 ˚C in a vacuum oven and then collected for recycling adsorption.

2.4. Adsorption kinetic and isothermal models

To study the adsorption kinetics, we used the following pseudo-first order (Eq. (4)) [34] and pseudo-second order (Eq. (5)) models [35].

$$\ln(q_e - -q_t) = \ln q_e - -K_1 t \quad (4)$$

$$t/q_t = 1/(K_2 {q_e}^2) + t/q_e \quad (5)$$

where, q_t and q_e are the amounts (mg/g) of Ce^{3+}, La^{3+}, Zn^{2+} and Mg^{2+} adsorbed on HKUST-1 at time t (min) and the equilibrium. K_1 (L/min) and K_2 (g/(mg•min^{-1})) are the kinetic rate constants of the pseudo-first-order and pseudo-second-order models, respectively.

The Langmuir isotherm (Eq. (6)) [36] and Freundlich isotherm models (Eq. (7)) [37] were used to study the adsorption isotherms.

$$C_e/q_e = 1/(qb) + C_e/q \quad (6)$$

$$\ln q_e = \ln K_f + (1/n) \times \ln C_e \quad (7)$$

where, q_e is the equilibrium adsorption (mg/g) of Ce^{3+}, La^{3+}, Zn^{2+} and Mg^{2+} on HKUST-1, and C_e is their equilibrium concentration (mg/L) in solution. q is the maximum adsorption capacity (mg/g) of the adsorbent, and b is the Langmuir constant. K_f is the Freundlich constant and n is a dependence degree of the adsorption capacity with the equilibrium concentration.

3. Results and discussion

3.1. Materials properties and structure characterizations

The X-ray diffraction patterns of the fresh HKUST-1 and regenerated samples are compared in Fig. 1a. The diffraction peaks can be indexed to HKUST-1 MOF [30]. However, the intensities of the diffrac-

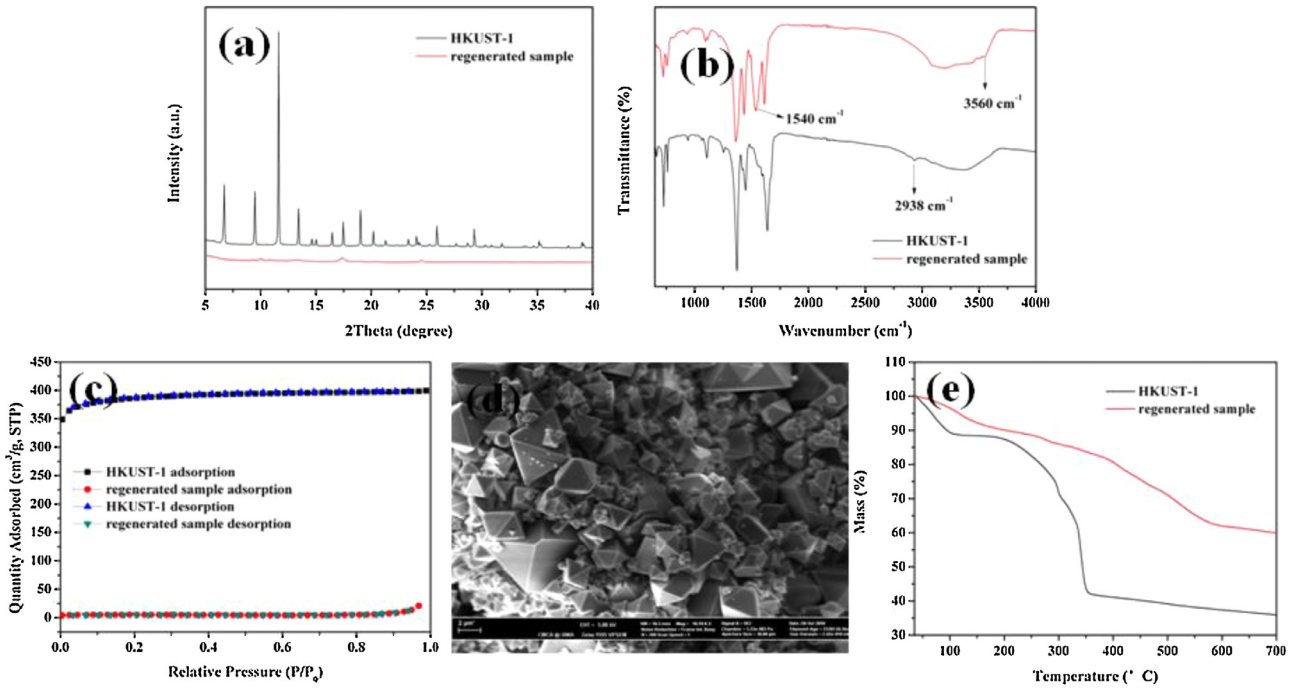

Fig. 1. Structure and properties of fresh and regenerated HKUST-1 MOFs. (a) XRD profiles, (b) FT-IR spectra, (c) N_2 adsorption/desorption isotherms, (d) SEM image, and (e) TGA profiles.

Table 1
The parameters of porous structure of HKUST-1 samples.

Adsorbent	Surface area (m^2/g) Langmuir	BET	Mean pore diameter (nm)	Total pore volume (cm^3/g)
Fresh	1740	1187	2.1	0.61
Regenerated sample	28	15	4.2	0.02

tion peaks from the regenerated sample are weaker than those of the fresh one, which should be due to the influence of adsorbed metal ions. Fig. 1b shows the FT-IR spectra of the fresh HKUST-1 and the regenerated samples. The characteristic peak of HKUST-1 at 724 cm^{-1} is attributed to Cu-O bond confirming the metal-linker coordination [31]. Also, the bands at 1370 cm^{-1} and 1450 cm^{-1} are assigned to the C–O of H_3BTC and C=O of H_3BTC, respectively. The broad peak formation at 3128 - 3656 cm^{-1} indicated the presence of water molecules in HKUST-1. After adsorption, the peak at 1110 cm^{-1} became a double-peak structure and the peak at 2938 cm^{-1} disappeared, suggesting that the host-guest interacted between HKUST-1 and metal ions. At the same time, the emerging characteristic peaks at 1540 and 3560 cm^{-1} confirmed that Ce^{3+} and La^{3+} were introduced into the HKUST-1 skeleton structure [38,39]. Furthermore, the bonds of Cu-O-Ce and Cu-O-La were possibly formed.

The nitrogen adsorption-desorption isotherms of the fresh and regenerated HKUST-1 samples are shown in Fig. 1c and Table 1 summarizes the textural properties. It can be seen that the isotherm of HKUST-1 possesses the property of the Type I isotherm [15]. Compared to the parent MOF, the regenerated sample showed a decreased surface area and smaller total pore volume, indicating that the regeneration process is difficult or the adsorbed metal ions are not easily eluted. The morphology of HKUST-1 is shown in Fig. 1d, revealing the octahedral shape with clear edges, similar to most of the reported HKUST-1 MOF [30]. Fig. 1e displays the weight loss profiles of pristine and the regenerated samples. The major weight loss occurs at the second stage for both samples, attributing to the structural decomposition of organic linkers. It can be seen that the regenerated sample is more stable than HKUST-1. In addition, the higher residual weight on the regenerated sample confirms more metallic species in the sample and the new coordinate bonds, which is consistent with the FT-IR results.

SEM-EDS elemental mappings of fresh HKUST-1 and the regenerated samples are shown in Fig. 2. Fig. 2a displays the EDX spectrum and SEM-EDX elemental mapping images of pristine MOF, revealing that the compositional elements of C, O and Cu are uniformly distributed on HKUST-1. Fig. 2b shows some obvious changes in the regenerated sample. Ce^{3+}, La^{3+}, Zn^{2+}, Mg^{2+} were well distributed on the surface of HKUST-1, suggesting the successful adsorption of the metal ions on the adsorbent. However, the atomic contents of the metal ions were different, indicating that HKUST-1 has better affinities towards the REEs.

3.2. *Effect of solution pH on metal adsorption*

The REEs adsorption on HKUST-1 at varying solution pHs was investigated at 25 °C with the initial concentration of ions at 400 mg/L. Fig. 3a shows that the removal efficiencies of all the metal ions enhanced with the increased pH. The removal efficiency did not change significantly as reported in the previous investigations [40,41], which means that the main mechanism of the metal adsorption on HKUST-1 may not be attributed to the electrostatic interaction. Fig. S1 shows the zeta potential of HKUST-1 under different pH values. As the pH increased, the surface charge of HKUST-1 became more negative; the pH of isoelectric point for HKUST-1 is 6.1. However, the adsorbents in suspension have no electric charge but the adsorption capacity of REE is high at this pH, reconfirming that some other factors might affect the adsorption of REE on HKUST-1.

The removal efficiency of REEs was much higher than that of other metal ions. It can be inferred that HKUST-1 possesses a high selective

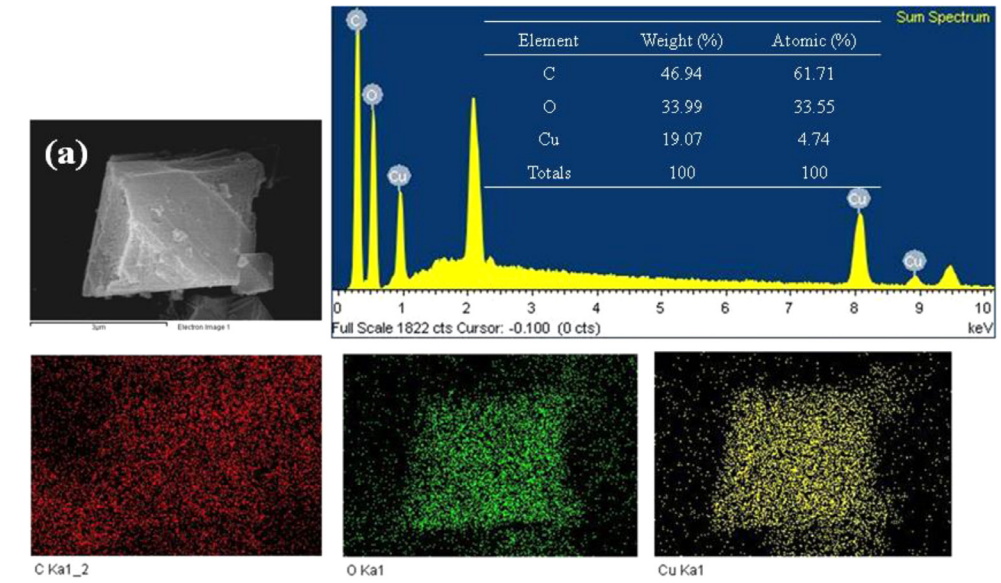

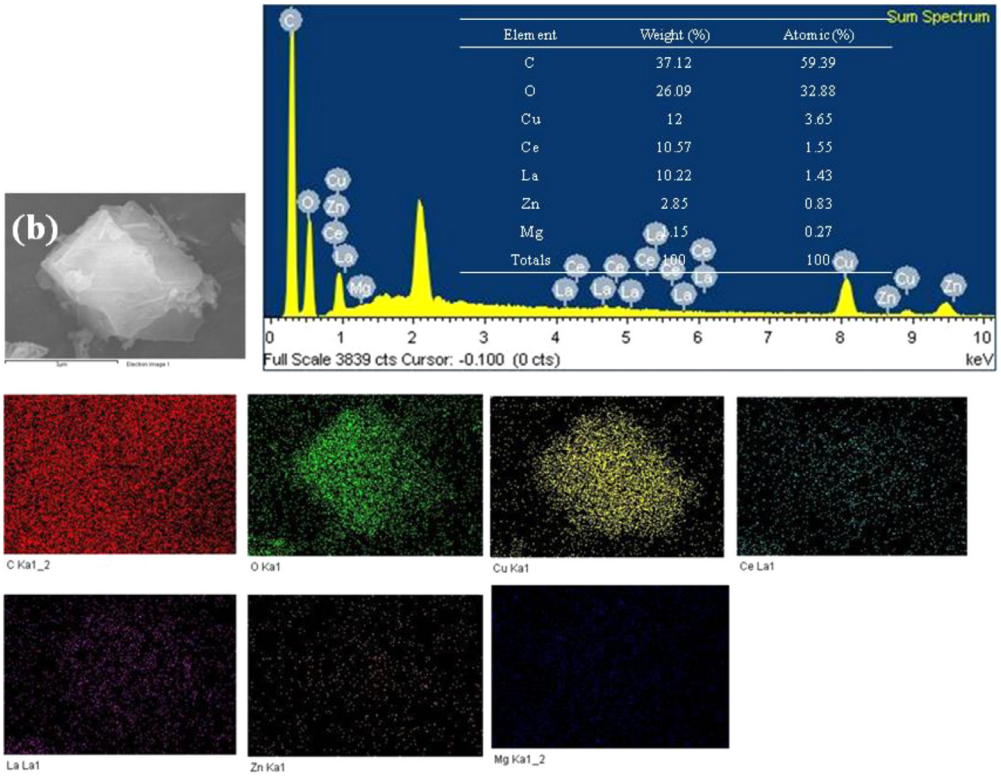

Fig. 2. SEM and EDX elemental distribution mapping analysis of HKUST-1 (a) and regenerated sample (b).

adsorption capacity for REEs. The equilibrium adsorption capacity and the selectivity of REEs are illustrated in Fig. 3b and c. Interestingly, the adsorption capacity between Ce^{3+} and La^{3+} was of a little difference, which can be attributed to the ion exchange and covalent bonding [39,42]. Fig. S2 shows the Cu^{2+} concentration for ion exchange with other metal ions in different solutions. The capacity of ion exchange of Cu^{2+} with other metal ions was very different. The ion exchange rate between Ce^{3+} and Cu^{2+} was weaker than that between La^{3+} and Cu^{2+}, but the exchange rate is much higher than that of Zn^{2+} and Mg^{2+}. Fig. 3d shows that solution pH significantly affected the stability of HKUST-1. With the increase of pH, Cu^{2+} concentration reduced to a much low value at pH 6. Therefore, pH = 6 was selected as the condition for further tests.

3.3. Adsorption kinetics and isotherms

Adsorption isotherms are of importance to the understanding of the interaction between adsorbent and adsorbate. Freundlich and Langmuir isotherm models were employed to depict the equilibrium data of the adsorption process. As shown in Fig. 4a and b that HKUST-1 presents a typical Freundlich isotherm, corresponding to heterogeneous adsorption sites with varying energies of adsorption [37]. The parameters of

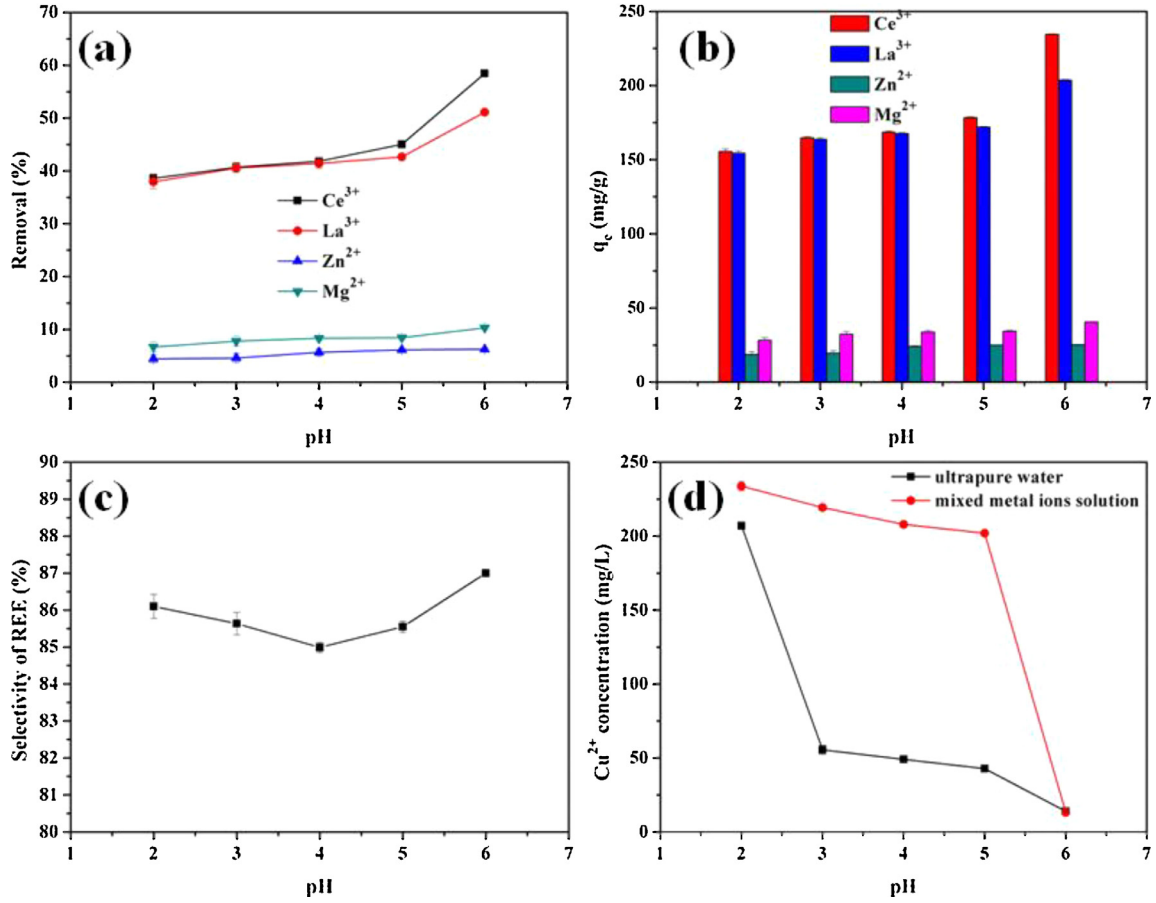

Fig. 3. Adsorption of La^{3+}, Ce^{3+}, Zn^{2+} and Mg^{2+} on HKUST-1 at varying pHs. (a) Removal efficiencies of different metal ions, (b) adsorption capacity, (c) selectivity of REE, and (d) concentrations of Cu^{2+} in ultrapure water and mixed metal ion solution. (C_0 = 400 mg/L, t = 480 min).

Table 2
The parameters of Freundlich and Langmuir adsorption isotherms of Ce^{3+} and La^{3+} on HKUST-1.

Metal	Langmuir model			Freundlich model		
	q (mg/g)	b	R^2	K_f	n	R^2
Ce^{3+}	558	0.004	0.982	28.8	2.43	0.994
La^{3+}	645	0.002	0.854	12.2	1.91	0.919

La^{3+} and Ce^{3+} adsorption isotherms are given in Table 2. It is seen that the correlation coefficients (R^2) of the Freundlich isotherm model for the two ions were 0.994 and 0.919, respectively, which were greater than those of the Langmuir model. Furthermore, the maximum adsorption capacity (q) for La^{3+} (645 mg/g) on HKUST-1 calculated using the Langmuir model was higher than Ce^{3+} (558 mg/g), which shows the similar tendency to the ion exchange (Fig. S2).

Toward the understanding of the adsorption kinetics of La^{3+} and Ce^{3+} on HKUST-1, the adsorption of La^{3+} and Ce^{3+} at different time was evaluated. The adsorption data are fitted by two kinetic models, pseudo-first-order and pseudo-second-order, to obtain the kinetic parameters. The linear curves of fitting to the two models are illustrated in Fig. 4c and d, demonstrating that the adsorption process can be better described by pseudo-second-order kinetics and the adsorption process is controlled by the chemical interaction. Table 3 lists the fitting kinetic rate constants. The pseudo-first-order kinetics do not well fit to the adsorption process due to the low correlation coefficients (R^2_{Ce3+} = 0.992, R^2_{La3+} = 0.969). Meanwhile, the pseudo-second-order model provides the correlation coefficients (R^2) at larger than 0.99 for Ce^{3+} and La^{3+} adsorption on HKUST-1. The calculated $q_{e\ Ce3+}$ (252 mg/g) and $q_{e\ La3+}$ (201 mg/g) are respectively close to the experimental $q_{e\ Ce3+}$ (234 mg/g) and $q_{e\ La3+}$ (203 mg/g) for the models of pseudo-second-order kinetics.

3.4. Effect of metal ions with different valence on REEs selective adsorption

To further confirm the selective adsorption of REEs on HKUST-1, metal ions with different valence states were introduced into the evaluation system. The equilibrium adsorption capacity and selectivity of REEs are illustrated in Fig. 5. Fig. 5a shows that HKUST-1 exhibits better selective adsorption capacities toward REEs than other metal ions, which is consistent with the findings in Section 3.2. When the solution pH value reached 6, the adsorption capacities of Ce^{3+}, La^{3+}, Co^{2+} and Cr^{3+} were 215 mg/g, 194 mg/g, 21 mg/g and 65 mg/g, respectively. This can be further proved by the fact that the performance of ion exchange and the covalent bonding between HKUST-1 and REEs are more favorable than that with other metal ions. Interestingly, the adsorption capacity of Cr^{3+} on HKUST-1 was better than that of Co^{2+}, because the high-valence cations have more favorable binding strengths with the active sites in HKUST-1 [43]. Fig. 5b displays the selectivity of REEs on HKUST-1 at varying solution pH. When the solution pH reached 6, the selectivity of REEs on HKUST-1 was 82.6%. Therefore, HKUST-1 still attained a high adsorption selectivity for REEs in the presence of other metal ions with different valent states.

Table 4 displays the performance comparison of the different adsorbents used for selective recovery of Ce^{3+} and La^{3+}. Compared with other MOF adsorbents, HKUST-1 shows a higher adsorption capacity and better selectivity, indicating that HKUST-1 is more suitable for adsorptive removals of La^{3+} and Ce^{3+} [44,45].

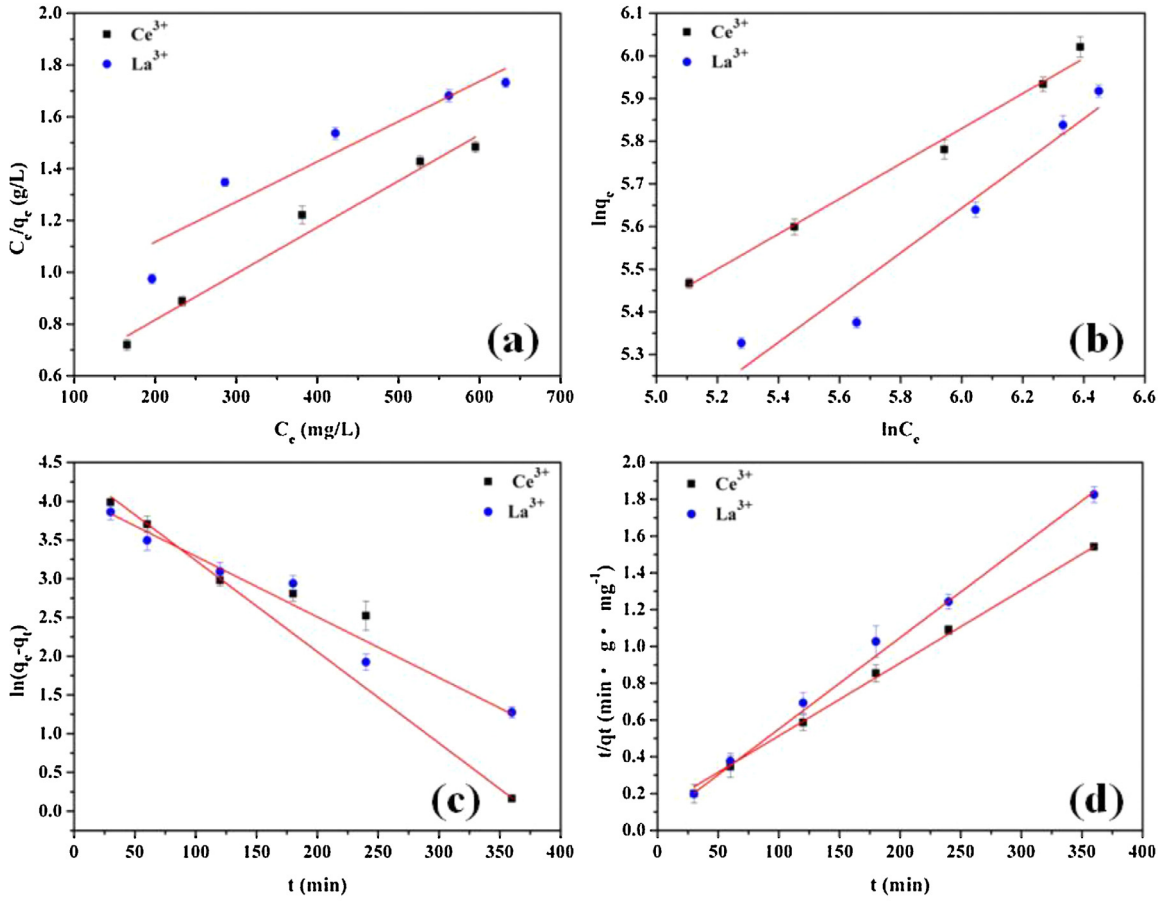

Fig. 4. Linear modeling of kinetics and isotherms of Ce^{3+} and La^{3+} adsorption. (a) Langmuir model, (b) Freundlich model, (c) Pseudo-first order kinetic and (d) Pseudo-second order kinetic models.

Table 3
Pseudo-first and pseudo-second order model parameters of Ce^{3+} and La^{3+} adsorption on HKUST-1.

Metal	$(q_e)_{Exp.}$ (mg/g)	Pseudo-first order			Pseudo-second order		
		$(q_e)_{Cal.}$ (mg/g)	K_1 (min^{-1})	R^2	$(q_e)_{Cal.}$ (mg/g)	K_2 (mg/g min)	R^2
Ce^{3+}	234	82	0.0117	0.992	252	0.00013	0.999
La^{3+}	203	58	0.0078	0.969	201	0.00045	0.998

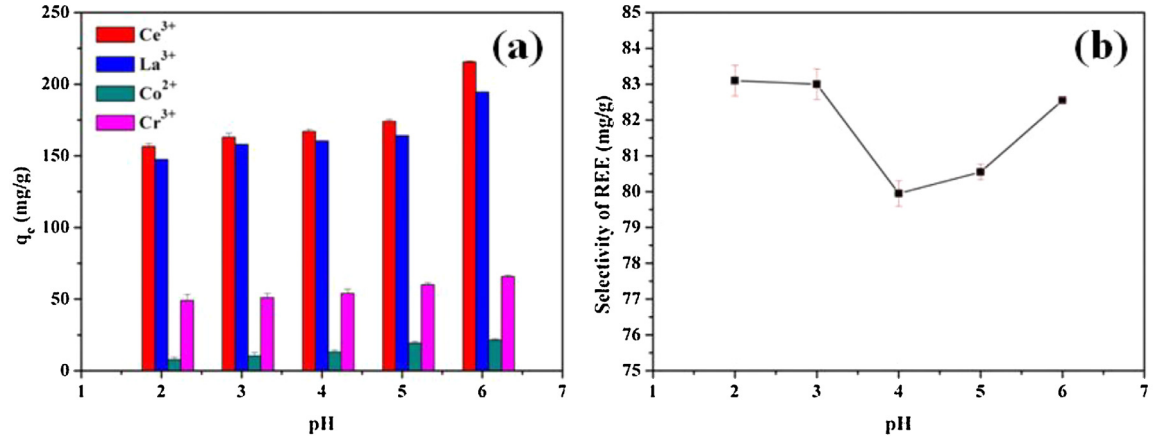

Fig. 5. Adsorption of Ce^{3+}, La^{3+}, Co^{2+} and Cr^{3+} on HKUST-1 at different pH values. (a) adsorption capacity and (b) selectivity of REE. (C_0 = 400 mg/L, t = 480 min).

Table 4
Comparison of the different adsorbents used for Ce^{3+} and La^{3+} selective recovery.

Adsorbent	Adsorption capacity of Ce^{3+} (mg/g)	Adsorption capacity of La^{3+} (mg/g)	Selectivity of Ce^{3+} and La^{3+} (%)	Reference
HKUST-1	234	203	87	This work
ZIF-8	—	385	—	[39]
MIL-101	11.3	14.6	33	[41]
MIL-101-DETA	52.8	39.7	31	[41]
MIL-101-PMIDA	48.3	37.2	28	[41]
Magnetite@MIL-101-SO_3	34.8	—	22	[44]
MOF-808-EDTA	—	200	—	[45]

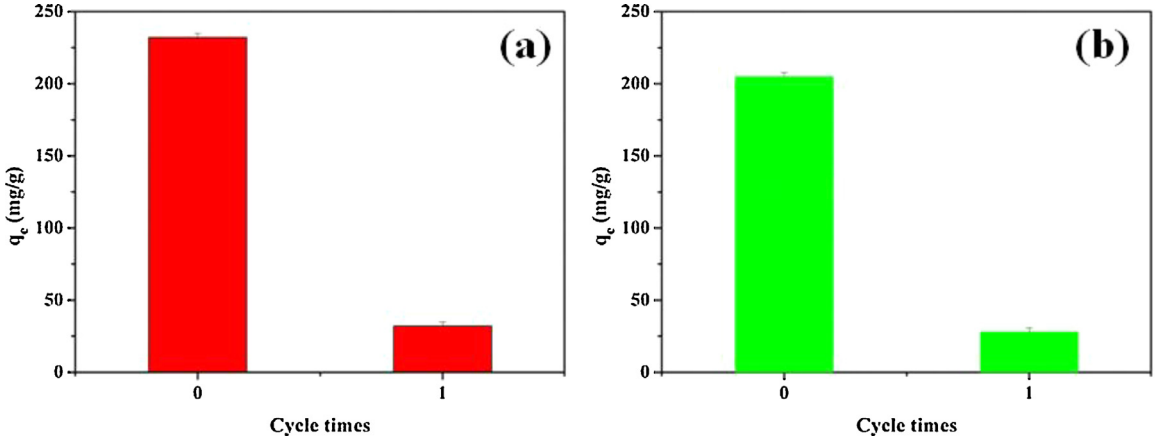

Fig. 6. Recycling use of HKUST-1 for Ce^{3+} (a) and La^{3+} (b) adsorption. (pH = 6, C_0 = 400 mg/g, and t = 480 min).

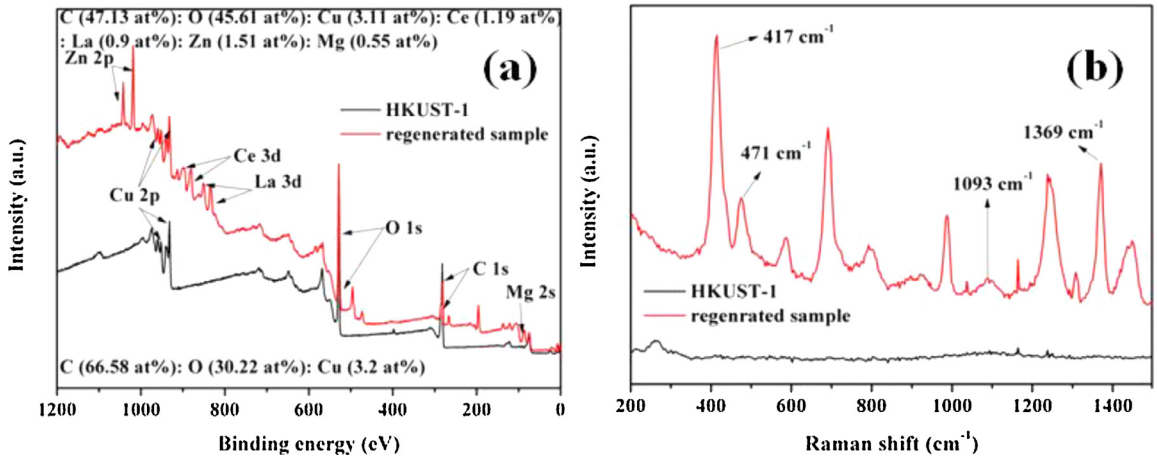

Fig. 7. (a) XPS survey spectrum and (b) Raman spectra of fresh and the regenerated HKUST-1 samples.

3.5. Reusability and adsorption mechanism

Reusability of the adsorbents was further tested in the recycle experiments (Fig. 6a and b). It was found that the adsorption capacity of Ce^{3+} and La^{3+} significantly decreased from 234 to 30 mg/g and from 203 to 26 mg/g after recycling HKUST-1 one time. Based on our previous study [34] and the findings in Section 3.2, it can be inferred that both ion exchange and the covalent bonding between metal ions and HKUST-1 play a role in the adsorption process. However, each metal ion possesses a different ability to form the covalent bond with HKUST-1 (such as Cu-O-La and Cu-O-Ce), which causes the selective adsorption between metal ions and the adsorbents. X-ray photoelectron spectroscopy (XPS) was employed to confirm the chemical environment. Fig. 7a gives the XPS full survey spectrum, indicating the presence of C, O and Cu elements with a small amount of Ce, La, Zn and Mg. It can be found that the binding energies of the Ce $3d_{3/2}$ and Ce $3d_{5/2}$ regions are 901.15 and 880.84 eV, the binding energies of the La $3d_{3/2}$ and La $3d_{5/2}$ regions are 850.37 and 832.06, respectively. As shown in Fig. 7b, Raman spectra were recorded to illustrate the vibrational properties of the fresh and used samples. It was shown that the observable peaks at 417, 471, 1093 and 1369 cm^{-1} are ascribed to ZnO [46], CeO_2 [47], La_2O_3 [48] and MgO [49], respectively, which reconfirm the intimate contacts between HKUST-1 and metal ions. The possible mechanism of the adsorption of rare earth ions on HKUST-1 is illustrated in Fig. S2.

4. Conclusions

In this work, HKUST-1 metal-organic framework was successfully developed for the selective adsorption of rare earth ions (Ce^{3+} and La^{3+}) from aqueous solutions. The adsorption process follows the Freundlich isotherm, while Langmuir isotherm presented the maximum adsorption capacity for Ce^{3+} and La^{3+} at 234 and 203 mg/g, respectively, at the optimum pH of 6 with C_0 = 400 mg/L. The selectivity toward rare earth ions was 87% among all the metal ions. In addition, the adsorption was

well fitted to a pseudo-second-order model. However, the recycled adsorbent displayed a reduced adsorption capacity. The adsorption mechanism of metal ions onto HKUST-1 follows ion exchange with covalent bonding. This study may contribute to the recovery of precious REEs by the development of novel porous adsorbents.

Acknowledgments

We acknowledge the financial support from the New Talent Training Plan (P173008052) from the State Administration of Foreign Experts Affairs of P. R. China. We also thank Mr Andrew Chan for his help in ICP-OES test. The supports of sample analysis from the Center for Microscopy, Characterization and Analysis, The University of Western Australia were also acknowledged.

Supplementary materials

Supplementary material associated with this article can be found, in the online version, at doi:10.1016/j.ceja.2020.100009.

References

[1] D.C. Li, S.B. Huang, W.H. Wang, A. Peng, Study on the kinetics of cerium (III) adsorption-desorption on different soils of China, Chemosphere 44 (2001) 663–669.
[2] S.F. Xue, W.Y. Wu, X. Bian, Y.F. Wu, Dehydration, hydrolysis and oxidation of cerium chloride heptahydrate in air atmosphere, J. Rare Earths 35 (2017) 1156–1163.
[3] X.Q. Sun, H.M. Luo, S.M. Mahurin, R. Liu, X.S. Hou, S. Dai, Adsoprtion of rare earth ions using carbonized polydopamine nanocarbon shells, J. Rare Earths 34 (2016) 77–82.
[4] P. Maestro, D. Huguenin, Industrial applications of rare earths: which way for the end of the century, J. Alloys. Compd. 225 (1995) 520–528.
[5] B.S. Soller, S. Salzinger, B. Rieger, Rare earth metal-mediated precision polymerization of vinylphosphonates and conjugated nitrogen-containing vinyl monomers, Chem. Rev. 116 (2016) 1993–2022.
[6] Y. Kanazawa, M. Kamitani, Rare earth minerals and resources in the world, J. Alloys Compd. 37 (2006) 1339–1343.
[7] R.A. Chi, J. Tian, Z.J. Li, C. Peng, Y.X. Wu, S.R. Li, C.W. Wang, Z.A. Zhou, Existing state and partitioning of rare earth on weathered ores, J. Rare Earths 23 (2005) 756–759.
[8] J. Tian, J.Q. Yin, R.A. Chi, G.H. Rao, M.T. Jiang, K.X. O.-Yang, Kinetics on leaching rare earth from the weathered crust elution-deposited rare earth ores with amonium sulfate solution, Hydrometallurgy 101 (2010) 166–170.
[9] D.M. Park, A. Brewer, D.W. Reed, L.N. Lammers, Y.Q. Jiao, Recovery of rare earth elements from low-grade feedstock leachates using engineered bacteria, Environ. Sci. Technol. 51 (2017) 13471–13480.
[10] S.X. Wu, L.S. Wang, L.S. Zhao, P. Zhang, H. E.-Shall, B. Moudgil, X.W. Huang, L.F. Zhang, Recovery of rare earth elements from phosphate rock by hydrometallurgical processes-A critical review, Chem. Eng. J. 335 (2018) 774–800.
[11] Z.Y. Zhao, X.Q. Sun, Y.M. Dong, Synergistic effect of doped functionalized ionic liquids in silica hybrid material for rare earth adsorption, Ind. Eng. Chem. Res. 55 (2016) 2221–2229.
[12] Y.Q. Gao, S.M. Zhang, K.Y. Zhao, Z.W. Wang, S.X. Xu, Z.P. Liang, K. Wu, Adsorption of La^{3+} and Ce^{3+} by poly-γ-glutamic acid crosslinked with polyvinyl alcohol, J. Rare Earths 33 (2015) 884–891.
[13] X.-.S. Wang, S.Q. Ma, D.F. Sun, S. Parkin, H.-.C. Zhou, A mesoporous metal-organic framework with permanent porosity, J. Am. Chem. Soc. 128 (2006) 16474–16475.
[14] J.D. Evans, B. Garai, H. Reinsch, W.J. Li, S. Dissegna, V. Bon, I. Senkovska, R.A. Fischer, S. Kaskel, C. Janiak, N. Stock, D. Volkmer, Metal-organic frameworks in Germany: from synthesis to function, Coord. Chem. Rev. 380 (2019) 378–418.
[15] X.L. Yan, S. Komarneni, Z.Q. Zhang, Z.F. Yan, Extremely enhanced CO_2 uptake by HKUST-1 metal-organic framework via a simple chemical treatment, Microporous Mesoporous Mater. 183 (2014) 69–73.
[16] R.-.B. Lin, S.C. Xiang, H.B. Xing, W. Zhou, B.L. Chen, Exploration of porous metal-organic frameworks for gas separation and purification, Coord. Chem. Rev. 378 (2019) 87–103.
[17] Y.F. Yue, J.A. Rabone, H.J. Liu, S.M. Mahurin, M.R. Li, H.L. Wang, Z.L. Lu, B.L. Chen, J.H. Wang, Y.X. Fang, S. Dai, A flexible metal-organic framework: guest molecules controlled dynamic gas adsorption, J. Phys. Chem. C 119 (2015) 9442–9449.
[18] B.Q. Lei, M.F. Wang, Z.L. Jiang, W. Qi, R.X. Su, Z.M. He, Constructing redox-responsive metal-organic framework nanocarriers for anticancer drug delivery, ACS Appl. Mater. Interfaces 10 (2018) 16698–16706.
[19] S. Rojas, I. Colinet, D. Cunha, T. Hidalgo, F. Salles, C. Serre, N. Guillou, P. Horcajada, Toward understanding drug incorporation and delivery from biocompatible metal-organic frameworks inview of cutaneous administration, ACS Omega 3 (2018) 2994–3003.
[20] L. Zhang, Y. Chen, R. Shi, T.G. Kang, G.S. Pang, B.R. Wang, Y. Zhao, X. Zeng, C.X. Zou, P. Wu, J.Y. Li, Synthesis of hollow nanocages MOF-5 as drug delivery vehicle to solve the load-bearing problem of insoluble antitumor drug oleanolic acid (OA), Inorg. Chem. Commun. 96 (2018) 20–23.
[21] Y.B. Dou, H. Zhang, A.W. Zhou, F. Yang, L. Shu, Y.B. She, J.R. Li, Highly efficient catalytic esterification in an $-SO_3H$-functionalized Cr (III)-MOF, Ind. Eng. Chem. Res. 57 (2018) 8388–8395.
[22] B. Li, A novel metal-organic framework as a heterogeneous catalysis for the solvent-free conversion of CO_2 and epoxides into cyclic carbonate, Inorg. Chem. Commun. 88 (2018) 56–59.
[23] M.M. Zhang, J.C. Guan, B.S. Zhang, D.S. Su, C.T. Williams, C.H. Liang, Chemical vapor deposition of Pd (C_3H_5) (C_5H_5) to synthesize Pd@MOF-5 catalysts for suzuki coupling reaction, Catal. Lett. 142 (2012) 313–318.
[24] D. Masih, V. Chernikova, O. Shekhah, M. Eddaoudi, O.F. Mohammed, Zeolite-like metal-organic framework (MOF) encaged Pt (II)-porphyrin for anion-selective sensing, ACS Appl. Mater. Interfaces 10 (2018) 11399–11405.
[25] F.Q. Wang, K.H. Xu, Z. Jiang, T. Yan, C.M. Wang, Y.Y. Pu, Y.N. Zhao, A multifunctional zinc-based metal-organic framework for sensing and photocatalytic applications, J. Lumin. 194 (2018) 22–28.
[26] P. Kumar, A. Deep, A.K. Paul, L.M. Bharadwaj, Bioconjugation of MOF-5 for molecular sensing, J. Porous Mater 21 (2014) 99–104.
[27] Y. Huang, X.F. Zeng, L.L. Guo, J.H. Lan, L.L. Zhang, D.P. Cao, Heavy metal ion removal of wastewater by zeolite-imidazolate frameworks, Sep. Purif. Technol. 194 (2018) 462–469.
[28] J. Li, X.X. Wang, G.X. Zhao, C.L. Chen, Z.F. Chai, A. Alsaedi, T. Hayat, X.K. Wang, Metal-organic framework-based materials: superior adsorbents for the capture of toxic and radioactive metal ions, Chem. Soc. Rev. 47 (2018) 2322–2356.
[29] N. Yin, K. Wang, Y.A. Xia, Z.Q. Li, Novel melamine modified metal-organic frameworks for remarkably high removal of heavy metal Pb (II), Desalination 430 (2018) 120–127.
[30] A. Malcki, B. Hayati, M. Naghizadch, S.W. Joo, Adsorption of hexavalent chromium by metal organic frameworks from aqueous solution, J. Ind. Eng. Chem. 28 (2015) 211–216.
[31] M.R. Azhar, H.R. Abid, H.Q. Sun, V. Periasamy, M.O. Tadé, S.B. Wang, One-pot synthesis of binary metal organic frameworks (HKUST-1 and UiO-66) for enhanced adsorptive removal of water contaminants, J. Colloid Interface Sci 490 (2017) 685–694.
[32] F. Zou, R.H. Yu, R.G. Li, W. Li, Microwave-assisted synthesis of HKUST-1 and functionalized HKUST-1-@$H_3PW_{12}O_{40}$: selective adsorption of heavy metal ions in water analyzed with synchrotron radiation, Chem. Phys. Chem 14 (2013) 2825–2832.
[33] L. Zhao, M.R. Azhar, X.J. Li, X.G. Duan, H.Q. Sun, S.B. Wang, X.C. Fang, Adsorption of cerium (III) by HKUST-1 metal-organic framework from aqueous solution, J. Colloid Interface Sci. 542 (2019) 421–428.
[34] M. Cheng, G.M. Zeng, D.L. Huang, C. Lai, Y. Liu, C. Zhang, R.Z. Wang, L. Qin, W.J. Xue, B. Song, S.J. Ye, H. Yi, High adsorption of methylene blue by salicylic acid-methanol modified steel converter slag and evaluation of its mechanism, J. Colloid Interface Sci. 515 (2018) 232–239.
[35] Y.S. Ho, G. Mckay, Pseudo-second order model for sorption processes, Process Biochem. 34 (1999) 451–465.
[36] I. Langmuir, The constitution and fundamental properties of solids and liquids. Part I. Solids, J. Am. Chem. Soc. 38 (1916) 2221–2295.
[37] H.M.F. Freundlich, Über die adsorption in Lasungen, Z. Phys. Chem. Leipz. 57A (1906) 385–470.
[38] M.M. Peng, M. Ganesh, R. Vinodh, M. Palanichamy, H.T. Jang, Solvent free oxidation of ethylbenzene over Ce-BTC MOF, Arab. J. Chem. 7 (2014) 1–7.
[39] L. Jiang, W. Zhang, C.G. Luo, D.J. Cheng, J.Q. Zhu, Adsorption toward trivalent rare earth element from aqueous solution by zeolitic imidazolate frameworks, Ind. Eng. Chem. Res. 55 (2016) 6365–6372.
[40] C. Lin, W.J. Luo, J.D. Chen, Q. Zhou, Rice husk grafted PMAA by ATRP in aqueous phase and its adsorption for Ce^{3+}, Chem. Phys. Lett. 690 (2017) 68–73.
[41] Y.R. Lee, K. Yu, S. Ravi, W.S. Ahn, Selective adsorption of rare earth elements over functionalized Cr-MIL-101, ACS Appl. Mater. Interfaces 10 (2018) 23918–23927.
[42] K.Y.A. Lin, Y.T. Hsieh, Copper-based metal organic framework (MOF), HKUST-1, as an efficient adsorbent to remove p-nitrophnol from water, J. Taiwan Inst. Chem. Eng. 50 (2015) 223–228.
[43] F. Zhao, E. Repo, Y. Song, D. Yin, S.B. Hammouda, L. Chen, S. Kalliola, J. Tang, K.C. Tam, M. Sillanpää, Polyethylenimine-cross-linked cellulose nanocrystals for highly efficient recovery of rare earth elements from water and a mechanism study, Green Chem. 19 (2017) 4816–4828.
[44] S.K. Elsaidi, M.A. Sinnwell, A. Devaraj, T.C. Droubay, Z. Nie, V. Murugesan, B.P. McGrail, P.K. Thallapally, Extraction of rare earth elements using magnetite@MOF composites, J. Mater. Chem. A 6 (2018) 18438–18443.
[45] Y.G. Peng, H.L. Huang, Y.X. Zhang, C.F. Kang, S.M. Chen, L. Song, D.H. Liu, C.L. Zhong, A versatile MOF-based trap for heavy metal ion capture and dispersion, Nat. Commun. 9 (2018) 1–9.
[46] R. Zhang, P.-.G. Yin, N. Wang, L. Guo, Photoluminescence and Raman scattering of ZnO nanorods, Solid State Sci. 11 (2009) 865–869.
[47] J.M. Zamaro, N.C. Pérez, E.E. Miró, C. Casado, B. Seoane, C. Téllez, J. Coronas, M.O.F. HKUST-1, A matrix to synthesize CuO and CuO-CeO_2 nanoparticle catalysts for CO oxidation, Chem. Eng. J. 195-196 (2012) 180–187.
[48] S.I. Boldish, W.B. White, Vibrational spectra of crystals with the A-type rare earth oxide structure-I. La_2O_3 and Nd_2O_3, Spectrochim. Acta Part A 35 (1979) 1235–1242.
[49] L. Kumari, W.Z. Li, C.H. Vannoy, R.M. Leblanc, D.Z. Wang, Synthesis, characterization and optical properties of $Mg(OH)_2$ micro-/nanostructure and its conversion to MgO, Ceram. Int. 35 (2009) 3355–3364.